Department of Applied Mechanics
STANFORD UNIVERSITY

Technical Report No. 193

WAVE FRONT ANALYSIS IN COMPOSITE MATERIALS

By

T.C.T. Ting
and
E.H. Lee

December 1968

Sponsored jointly by
ARPA Materials Research Council,
and
the Ballistic Research Laboratories on
Contract DA-04-200-AMC-659(X)
with Stanford University

Department of Applied Mechanics
STANFORD UNIVERSITY

Technical Report No. 193

WAVE FRONT ANALYSIS IN COMPOSITE MATERIALS

By

T.C.T. Ting
and
E.H. Lee

December 1968

Sponsored jointly by
ARPA Materials Research Council,
and
the Ballistic Research Laboratories on
Contract DA-04-200-AMC-659(X)
with Stanford University

WAVE FRONT ANALYSIS IN COMPOSITE MATERIALS

by

T.C.T. Ting* and E.H. Lee**

ABSTRACT

The propagation of an initially sharp plane pressure pulse through a linear elastic composite medium is analysed. Wave front and ray theory analogous to geometrical optics is shown to determine the change in shape of the leading wave front and also the stresses immediately behind it. For certain circumstances the stress amplitudes on this front, or the corresponding tensile stresses on its reflection at the free back surface of a slab, may be critical in design. Examples are presented of an initially sharp plane pressure pulse transmitted through an elastic circular cylinder and an elastic spherical inclusion. The method can be applied to more general composite configurations, and can be extended to determine the stress gradient behind the front. For the latter, general formulae are derived by which the reflection and transmission coefficients can be determined for the stress gradient and the higher order derivatives at an arbitrary interface.

---

* Associate Professor of Applied Mechanics, Dept. of Materials Engineering, Univ. of Illinois at Chicago Circle, Chicago, Illinois 60680.

** Professor, Dept. of Applied Mechanics, Stanford University, Stanford, Calif. 94305.

1. Introduction.

The damage which an initially plane compressive stress pulse can create when passing through a slab of composite material will depend on the attenuation of the pulse due to absorption and scattering, and this influence on the tensile stresses associated with reflection at the back free surface of the slab which can cause fracture and spalling. Few analytical investigations of such situations appear to have been carried out, and we therefore present a study which provides information on certain aspects of the phenomenon. In particular, we consider the variation in shape and stress magnitude of the wave-front as it traverses, for instance, a regular array of parallel cylindrical rods embedded parallel to the wave front, as depicted in Fig. 1a. The analysis is based on linear elastic response, and the reinforcing rods are considered to have different elastic constants and different density from those of the matrix. Attenuation of the stress wave then arises from refraction and reflection and the associated generation of shear waves. The shape of the front ceases to be plane, and this, as well as the attenuation, influences the tensile stress magnitudes caused by reflection at the back free surface. The analysis presented here applies to general three-dimensional wave propagation with inclusions of arbitrary shapes, although the examples given involve only two space variables for illustrative purposes.

We consider an initial wave as shown in Fig. 1b with a discontinuous rise in stress normal to the wave front of magnitude σ_o from the unstressed state ahead of the wave. Behind the front

the stress is considered to decrease gradually. Whether subsequently the stresses at the wave front are critical from the damage standpoint depends on the detailed structure of the composite medium, the properties of its components, and the width of the slab. It can happen that redistribution of the energy in the wave leads to concentration of stress well behind the wave front, and the present approach would then not elucidate the dominant mode of failure. The present solution indicates when the wave front will be sufficiently attenuated for this circumstance.

The basis for the present approach is the ray tracing and associated wave front analysis of geometric optics [1-5]. It can be shown that even in the case of elastic waves with two basic wave speeds in each material, the stress amplitude at the initial wave front is given exactly by the laws of geometrical optics associated with the propagation of irrotational waves. This follows from application of the theory of characteristics and is in accord with the more common interpretation of geometrical optics as an approximation to the solution for oscillatory waves at high frequencies. This approach determines the stress tensor at the wave front, and can be extended also to determine stress gradients there.

It is well known that the displacement vector $\underset{\sim}{u}$ for dynamic analysis of an isotropic linear elastic body can be expressed in terms of the scalar potential Φ and the vector potential $\underset{\sim}{\Psi}$ in the form

$$\underset{\sim}{u} = \nabla\Phi + \nabla \times \underset{\sim}{\Psi} \qquad (1)$$

where Φ and $\underset{\sim}{\Psi}$ satisfy the following equations

$$\nabla^2\Phi = \frac{1}{\alpha^2}\frac{\partial^2\Phi}{\partial t^2} \quad , \quad \alpha^2 = (\lambda+2\mu)/\rho \tag{2}$$

$$\nabla^2\underset{\sim}{\Psi} = \frac{1}{\beta^2}\frac{\partial^2\underset{\sim}{\Psi}}{\partial t^2} \quad , \quad \beta^2 = \mu/\rho \tag{3}$$

$$\nabla\cdot\underset{\sim}{\Psi} = 0 \tag{4}$$

λ and μ are Lame's constants and ρ is the density of the material. Since $\alpha > \beta$, the scalar potential Φ is governed by a wave equation with a greater wave velocity, and hence for a wave moving into an undisturbed medium, the region adjacent to the leading wave front corresponds to zero $\underset{\sim}{\Psi}$, until the slower distortion wave arrives. This follows from the "region of influence" theory of the solutions of hyperbolic equations [6]. Therefore $\underset{\sim}{u} = \nabla\Phi$ behind the wave front. Let (ξ_1,ξ_2,ξ_3) be a system of orthogonal coordinates with ξ_1 normal to the wave fronts. Thus ξ_1 = constant is the front of the disturbance. If we consider Φ to be zero in the undisturbed region ahead of the front, Φ is also zero immediately behind the front. Since displacements must be continuous in an elastic body, $\underset{\sim}{u} = \nabla\Phi = 0$ immediately behind the wave front. This, together with the fact that $\Phi = 0$ at the wave front gives

$$\frac{\partial^2\Phi}{\partial\xi_i\partial\xi_j} = 0, \text{ except for } i=j=1 .$$

Accordingly, the only non-vanishing strain component immediately behind the wave front is ϵ_{11}. For this simple one-dimensional strain, the stresses can be written down immediately using Hook's law:

$$\sigma_{11} = (\lambda+2\mu)\epsilon_{11} , \quad \sigma_{22} = \sigma_{33} = \lambda\epsilon_{11}$$

$$\sigma_{12} = \sigma_{23} = \sigma_{13} = 0 . \tag{5}$$

Introducing the average hydrostatic tension

$$p = \sigma_{ii}/3 = (\lambda + \frac{2}{3}\mu)\epsilon_{ii} = (\lambda + \frac{2}{3}\mu)\nabla^2\Phi , \tag{6}$$

since $\epsilon_{ii} = \epsilon_{11}$ in the present case, Eq. (5) is reduced to,

$$\sigma_{11} = \frac{\lambda+2\mu}{3\lambda+2\mu} 3p , \quad \sigma_{22} = \sigma_{33} = \frac{\lambda}{3\lambda+2\mu} 3p$$

$$\sigma_{12} = \sigma_{23} = \sigma_{13} = 0 \tag{7}$$

Thus it suffices to study the propagation of p, or $\nabla^2\Phi$ by Eq. (6), which satisfies the acoustic wave equation (2), in order to determine the variation of stress generated by the passage of the wave front. The problem therefore is reduced to acoustic wave analysis with a single wave velocity as for a gas, and the conditions immediately behind the wave front can be determined by geometrical acoustics for the single scalar wave equation.

2. Geometrical Acoustics.

Ray tracing and wave-front analysis for the scalar wave equation has been termed "geometrical acoustics" by Friedlander [2] in a detailed presentation of the topic. He developes the theory of characteristics and shows that wave fronts as they vary in time form a three-dimensional characteristic manifold in four dimensional space-time. If $t = \tau(\underset{\sim}{x})$ is the equation for the wave front at time t, it is known that $\tau(\underset{\sim}{x})$ satisfies the eikonal equation

$$(\nabla\tau) \cdot (\nabla\tau) = \frac{1}{\alpha^2} \tag{8}$$

The rays normal to these fronts are bi-characteristics, and a system of ordinary differential equations governs conditions along each ray. The propagation of discontinuities is considered through the analysis of "weak solutions" of the wave equation using the theory of distributions or generalized functions [3]. It is shown that the saltus or jump across a discontinuity satisfies:

$$2(\nabla\tau) \cdot \nabla[p] + [p]\nabla^2\tau = 0 \tag{9}$$

which Luneburg [1] called the transport equation. $[p]$ stands for the saltus which is identical to p behind the wave front in the present case, since p is zero ahead of the wave front. The transport equation (9) can be reduced to an ordinary differential equation along the ray and yields, when integrated, the intensity law of geometrical optics, that the energy density integrated across a tube of rays

remains constant. For propagation through a homogeneous medium, the energy can be represented by the square of the hydrostatic tension p, so that p varies inversely as the square root of the area of cross section of the ray tube. For a homogeneous medium the rays are straight, so that the area of an infinitesimal ray tube is given directly in terms of the Gaussian curvature of the wave front. If R and S are the principal radii of curvature at the wave front, we have

$$p^2RS = \text{constant} \tag{10a}$$

along the ray. If one of the radii, say S, is infinite as in the case of two-dimensional wave motions, we have, instead of (10a)

$$p^2R = \text{constant} \tag{10b}$$

Changes in intensity at the boundary between the matrix and inclusions are determined by the equivalent of Fresnel's formulae for elastic media [7].

The above rules are identical with those used in classical geometrical optics and considered as an approximation to the propagation of high frequency waves. It was, we believe, first pointed out by Luneburg in the lecture notes which comprised the fore-runner of [1], that they express the propagation of a discontinuity exactly within the limits of linear theory. In the following two sections, we illustrate the method of geometrical acoustics by considering a plane sharp wave front of the type shown in Fig. 1b propagating through an elastic circular cylindrical inclusion. The case when the inclusion is a sphere

is discussed in Section 5. In Section 6, we derive the equations which enable one to determine the stress gradient and the higher order derivatives of stresses behind the wave front.

3. Geometry of the Wave Fronts.

Fig. 2 shows the wave front configurations generated when the plane incident wave interacts with an embedded reinforcing circular cylindrical inclusion. The ratio α_2/α_1 of the dilatation wave speed in the reinforcement (medium 2) to that in the matrix (medium 1) is taken to be $4/3$. As the wave front strikes the inclusion both refracted and reflected Φ and $\underset{\sim}{\Psi}$ waves are produced. As shown in Fig. 2a an incident wave thus produces four different wave fronts. The motion in the regions between the dilatation wave front (Φ) and the distortion wave front $(\underset{\sim}{\Psi})$ is irrotational because $\underset{\sim}{\Psi}$ is zero. However, this does not imply that shear stresses are zero. In view of symmetry, only upper-halves of the wave fronts are shown in the figure.

The wave fronts become more complicated when the incident wave front passes the point Q where total reflection of the dilatation wave occurs and the incident wave produces no refracted dilatation wave (Fig. 2b). For simplicity distortion wave fronts are omitted from this figure. Also omitted are the wave fronts due to multiple refractions and reflections except the precursor dilatation wave abcd in Figs. 2b and 2c. All rays which reach the wave front cd in Fig. 2b have undergone a single refraction, while the rays which reach the wave front ebc have been subjected to two refractions through the inclusion.

In the following our main interest will be the determination of the wave front abcd and the discontinuity in pressure at this wave front. Therefore, we need consider only those incident rays which meet the inclusion at points below Q. The reflected wave front ef can be determined in the same manner.

Although the wave fronts can be located by integrating Eq. (8), it is simpler by a direct calculation using Fermat's principle. To illustrate the procedure in computing rays and wave fronts, let us consider a ray AB in Fig. 3 which strikes the inclusion at angular position θ. If a is the radius of the inclusion, the coordinates of B are given by:

$$x_B = a(1-\cos\theta) \tag{11a}$$

$$y_B = a\sin\theta \tag{11b}$$

Let $t = 0$ be the time at which the initial plane wave reaches $x = 0$ and contacts the inclusion. Then the time t required for point C on the refracted ray BD to be reached by the wave front is

$$t = \frac{x_B}{\alpha_1} + \frac{\ell_{BC}}{\alpha_2}$$

or

$$\ell_{BC} = \alpha_2\left(t - \frac{x_B}{\alpha_1}\right) \tag{12}$$

where ℓ_{BC} is the length of the straight ray BC. The inclination of the refracted ray to the incident ray direction, δ, is given by Snell's law:

$$\frac{\sin(\theta + \delta)}{\sin\theta} = \frac{\alpha_2}{\alpha_1} \tag{13}$$

The coordinates of the point C are thus:

$$x_C = x_B + \ell_{BC}\cos\delta \tag{14a}$$

$$= a(1-\cos\theta) + \alpha_2\cos\delta\,[t - \frac{a}{\alpha_1}(1-\cos\theta)]$$

$$y_C = y_B + \ell_{BC}\sin\delta \tag{14b}$$

$$= a\sin\theta + \alpha_2\sin\delta\,[t - \frac{a}{\alpha_1}(1-\cos\theta)]$$

For a given t, (14a,b) is the equation for the wave front cd in Fig. 2b with θ as parameter. By direct calculation it can be shown that the slope of the front is perpendicular to the ray BC, as it must be according to Huygens' construction for wave fronts.

A similar calculation determines the wave front after refraction out of the inclusion. For the coordinates of point E in Fig. 3, we have

$$x_E = x_B + \ell_{BD}\cos\delta + \ell_{DE}\cos 2\delta \tag{15a}$$

$$y_E = y_B + \ell_{BD}\sin\delta + \ell_{DE}\sin 2\delta \tag{15b}$$

where

$$\ell_{BD} = 2a\cos(\theta+\delta) \tag{16}$$

and ℓ_{DE} is determined by

$$t = \frac{x_B}{\alpha_1} + \frac{\ell_{BD}}{\alpha_2} + \frac{\ell_{DE}}{\alpha_1}$$

or

$$\ell_{DE} = \alpha_1 t - x_B - \frac{\alpha_1}{\alpha_2} \ell_{BD} \tag{17}$$

Clearly, one can continue this procedure to determine the wave fronts if there is more than one inclusion.

The wave fronts as expressed by Eqs. (14a,b) and (15a,b) are shown in Fig. 3 for various times. The dotted line Qb is the locus of intersection of the initial incident plane wave front and the refracted wave front. The determination of the pressure p on the wave front will be described in the next section.

4. Stress Magnitudes at the Wave Front.

The change in magnitude of stresses due to refraction at point B or D in Fig. 3 should be independent of the curvatures of the incoming wave front and the interface. While this statement seems intuitively correct, there appear to be no proofs available. We will prove this in Section 6, and therefore we accept this fact as valid in this Section.

For a given plane dilatation wave Φ of magnitude A_1 incident on a plane interface, the refracted dilatation wave Φ' of magnitude A' has been determined in [7]. However, we are interested in p, and hence $\nabla^2\Phi$ by Eq. (6). If

$$\frac{\Phi'}{\Phi} = \frac{A'}{A_1}$$

at the interface, then according to [7],

$$\frac{\nabla^2\Phi'}{\nabla^2\Phi} = \frac{A'\alpha^2}{A_1\alpha'^2} \tag{18}$$

Making use of Eq. (6) and the result obtained in [7] for the value A'/A_1, we write the pressure ratio p'/p at the interface in the following form:

$$\frac{p'}{p} = F(\theta, \frac{\alpha'}{\alpha}, \frac{\beta}{\alpha}, \frac{\beta'}{\alpha'}, \frac{\rho'}{\rho})$$

$$= \frac{\rho'(\alpha'^2 - \frac{4}{3}\beta'^2)\alpha^2}{\rho(\alpha^2 - \frac{4}{3}\beta^2)\alpha'^2} \left(\frac{2\cos\theta M}{KM+LN}\right) \tag{19}$$

$$K = \cos\theta\left(\frac{\rho'}{\rho} + \eta\sin^2\theta\right) + \frac{\alpha}{\alpha'} \sqrt{1-\left(\frac{\alpha'}{\alpha}\sin\theta\right)^2}\ (1-\eta\sin^2\theta)$$

$$M = \left(\frac{\rho'}{\rho} + \eta\sin^2\theta\right) + \frac{\beta}{\beta'} \sqrt{\frac{1-\left(\frac{\beta'}{\alpha}\sin\theta\right)^2}{1-\left(\frac{\beta}{\alpha}\sin\theta\right)^2}}\ (1-\eta\sin^2\theta)$$

$$L = \frac{\beta}{\alpha} \frac{\sin\theta}{\sqrt{1-\left(\frac{\beta}{\alpha}\sin\theta\right)^2}}\ (1 - \frac{\rho'}{\rho} - \eta\sin^2\theta) - \frac{\alpha}{\alpha'}\eta\sin\theta \sqrt{1-\left(\frac{\alpha'}{\alpha}\sin\theta\right)^2}$$

$$N = (1 - \frac{\rho'}{\rho} - \eta\sin^2\theta)\sin\theta - \frac{\alpha}{\beta'}\eta\sin\theta\cos\theta \sqrt{1-\left(\frac{\beta'}{\alpha}\sin\theta\right)^2}$$

where

$$\eta = 2\left[\left(\frac{\beta}{\alpha}\right)^2 - \frac{\rho'}{\rho}\left(\frac{\beta'}{\alpha}\right)^2\right]$$

The quantities with a prime refer to the refracted medium while the quantities without a prime refer to the incident medium. The transmission coefficient as expressed by Eq. (19) has been tabulated in [8] for $\frac{\beta}{\alpha} = \frac{\beta'}{\alpha'} = 1/\sqrt{3}$ with variable θ, $\frac{\alpha'}{\alpha}$ and $\frac{\rho'}{\rho}$.

Let $(p_B)_2$ and $(p_B)_1$ be pressure at point B of Fig. 3 on the side of medium 2 and medium 1 respectively. Since $(p_B)_1 = p_o$, the incident constant pressure, $(p_B)_2$ can then be determined by using Eq. (19). The geometrical acoustics law Eq. (10b) then gives

$$\frac{p_C}{(p_B)_2} = \sqrt{\frac{(R_B)_2}{R_C}} \tag{20}$$

where $(R_B)_2$ is the radius of curvature of the wave front at the point B in medium 2, and R_C is the radius of curvature at C. Because the rays are straight lines normal to the wave front in each medium

$$R_C = (R_B)_2 + \ell_{BC} \tag{21}$$

and hence we can determine the pressure at any point in the inclusion. Although $(R_B)_2$ could be obtained by differentiation from the wave front expression (14), it is more convenient to analyse the refraction geometry adjacent to the point B.

Let us consider a more general situation as shown in Fig. 4 in which an incident ray OB strikes the interface boundary at B and

produces a refracted ray BC. Let R_i and R_r denote respectively the radii of curvature of the incident and refracted wave fronts at point B. Moreover let R_b denote the radius of curvature of the interface boundary at point B. By considering an adjacent incident ray OD, it can be shown that the following relation holds:

$$\cot\theta_i\left(\frac{\cos\theta_i}{R_i}+\frac{1}{R_b}\right) = \cot\theta_r\left(\frac{\cos\theta_r}{R_r}+\frac{1}{R_b}\right) \tag{22}$$

In Eq. (22), R_b assumes a negative value if the center of curvature of the interface is on the left of the boundary instead of on the right as shown in Fig. 4. Likewise, R_i and R_r can assume negative values.

Applying Eq. (22) to point B in Fig. 3, we obtain, since $R_i = \infty$, and using Snell's law, Eq. (13),

$$(R_B)_2 = \frac{a\cos^2(\theta+\delta)}{\frac{\alpha_2}{\alpha_1}\cos\theta-\cos(\theta+\delta)} \tag{23}$$

With Eqs. (21) and (23), Eq. (20) determines the pressure p at the wave front inside the inclusion. Figure 5 shows an example of the pressure p as a function of position when the wave front arrives. The results are shown in the form of contour lines of constant pressure. The material constants used are $\alpha_2/\alpha_1 = 4/3$, $\beta_1/\alpha_1 = \beta_2/\alpha_2 = 1/\sqrt{3}$ and $\rho_2/\rho_1 = 1$. The pressure at point O inside the inclusion is $1.142\ p_o$ and increases to $2.522\ p_o$ as Q is approached from O along the circumference of the inclusion. On the other hand, the pressure at H inside the inclusion is $0.885\ p_o$ and decreases to zero as we approach Q along the circumference. Thus Q is a point of singularity.

Figure 5 also shows the results of similar calculations for pressure at the wave front after refraction out of the inclusion. The pressure at H outside of the inclusion is $0.758\ p_o$ and decreases to zero as we approach Q along the outside of the circumference. The line Qe is the contour line for zero pressure. However, if we regard Qe as the reflected ray at Q and calculate the reflected pressure along Qe, we will find that the reflected pressure along Qe is not zero. Hence there is a discontinuity in pressure across Qe. In fact, the radius of curvature of the wave front feb of Fig. 2b which consists of the reflected front fe and the refracted front eb is discontinuous at e.

Figure 5, when used in conjunction with Fig. 3, enables one to determine the pressure at the wave front for a given time t. The wave fronts obtained in Fig. 3 are also shown in Fig. 5. Notice that the pressure in the region above the dotted line Qb is the pressure on the refracted wave front. The actual pressure should include the incident plane wave pressure p_o. The stresses at the wave front in this region should be modified accordingly.

The pressure along the x-axis has a simple form and is recorded here. Substituting $\theta = \delta = 0$ in Eq. (23), we have

$$R_{o^+} = \frac{a}{\frac{\alpha_2}{\alpha_1} - 1} \tag{24}$$

where the o^+ refers to the abscissa value of the point designated. Evaluation of (19) gives

$$p_{o+} = \frac{1 - \frac{4}{3}\left(\frac{\beta_2}{\alpha_2}\right)^2}{1 - \frac{4}{3}\left(\frac{\beta_1}{\alpha_1}\right)^2} \frac{2\frac{\rho_2}{\rho_1}}{\frac{\rho_2}{\rho_1} + \frac{\alpha_1}{\alpha_2}} p_o \tag{25}$$

and application of (20) yields

$$p(x) = (p_{o+}) \sqrt{\frac{a}{a + x(\frac{\alpha_2}{\alpha_1} - 1)}}, \quad 0 < x < 2a \tag{26}$$

Refraction out of the inclusion gives

$$R_{2a-} = 2R_{2a+} \tag{27}$$

and hence

$$p(x) = \frac{4p_o}{\left(2 + \frac{\rho_1\alpha_1}{\rho_2\alpha_2} + \frac{\rho_2\alpha_2}{\rho_1\alpha_1}\right)\sqrt{(2\frac{\alpha_2}{\alpha_1} - 1) + 2(\frac{x}{a} - 2)(\frac{\alpha_2}{\alpha_1} - 1)}}, \quad x > 2a \tag{28}$$

until the next reinforcing cylinder is reached. It is interesting to note that for $\alpha_2 > \alpha_1$, the usual case for composites, the wave fronts diverge and the stress amplitude attenuates. However, for $\alpha_2 < \alpha_1$, a converging wave front occurs after the first refraction, and the energy becomes concentrated at the caustic giving infinite stress values according to the linear theory. Stress concentration can occur also at the distortion wave front when $\beta_2 < \alpha_1$.

5. Wave Propagation through a Spherical Inclusion.

For an initial plane wave as shown in Fig. 1b propagating through a spherical inclusion of radius a, the geometry of the wave fronts

intersecting a plane through the axis of symmetry is the same as for the cylindrical inclusion shown in Fig. 3. Thus the results obtained in Section 3 apply equally well to a spherical inclusion if we replace y by r, the radial distance from the axis of symmetry x. The procedures outlined in Section 4 for determining the stress magnitude at the wave front are still applicable except that the intensity law Eq. (10a) should be used instead of Eq. (10b). Thus, Eq. (20) should be replaced by

$$\frac{p_C}{(p_B)_2} = \sqrt{\frac{(R_B)_2(S_B)_2}{R_C S_C}} \tag{29}$$

where

$$S_C = (S_B)_2 + \ell_{BC} \tag{30}$$

$$(S_B)_2 = \frac{a \sin\theta}{\sin\delta} \tag{31}$$

In Fig. 6, we show the pressure at the wave front for a spherical inclusion using the same material parameters as in Fig. 5 for comparison. Again, point Q is a point of singularity and the pressure suffers a jump across Qe. As is to be expected, more rapid attenuation of the wave front occurs for a spherical inclusion than for a cylindrical inclusion because of spreading in all directions parallel to the wave front, and the formulae for attenuation along the x-axis Eq. (26,28) are simply modified by removal of the square root since to second order the wave front is spherical by symmetry on this axis.

6. Stress Gradient and Higher Order Derivatives Behind the Wave Front.

To determine the spatial derivatives of stress right behind the wave front, we have to establish the higher order transport equations which determine the propagation of discontinuities in stress derivatives along the ray and an extension of the equivalent of Fresnel's formulae for the reflection and transmission coefficients of the stress derivatives at an interface. It should be noted that spacial derivatives and time derivatives of any quantity, say Φ, behind the wave front are related once we know Φ at the wave front. For, if $t = \tau(\underset{\sim}{x})$ is the wave front at time t, we have

$$\nabla\{\Phi(\underset{\sim}{x},\tau(\underset{\sim}{x}))\} = \{\nabla\Phi(\underset{\sim}{x},t)\}_{t=\tau(\underset{\sim}{x})} + \nabla\tau(\underset{\sim}{x})\,\{\frac{\partial}{\partial t}\Phi(\underset{\sim}{x},t)\}_{t=\tau(\underset{\sim}{x})} \qquad (32)$$

Similarly, the k-th order spatial derivative of Φ at the wave front, the limits being taken as the front is approached from behind which applies throughout this section, can be determined once we know the first k order time derivatives of Φ at the wave front. It suffices therefore to discuss the propagation of discontinuities in time derivatives.

Let $t = \tau(\underset{\sim}{x})$ and $t = \bar{\tau}(\underset{\sim}{x})$ be the dilatation and distortion wave fronts respectively at time t. Then $\tau(\underset{\sim}{x})$ and $\bar{\tau}(\underset{\sim}{x})$ satisfy the eikonal equations

$$(\nabla\tau)\cdot(\nabla\tau) = \frac{1}{\alpha^2} \qquad (33a)$$

$$(\nabla\bar{\tau})\cdot(\nabla\bar{\tau}) = \frac{1}{\beta^2} \qquad (33b)$$

Define

$$\zeta = t - \tau(\underset{\sim}{x}) \tag{34a}$$

$$\bar{\zeta} = t - \bar{\tau}(\underset{\sim}{x}) \tag{34b}$$

Physically, ζ and $\bar{\zeta}$ are the times elapsed after the arrival of the dilation and distortion wave fronts. At the dilatation wave front $\zeta = 0$ and at the distortion wave front $\bar{\zeta} = 0$. Now we expand Φ and $\underset{\sim}{\Psi}$ into the following series [2]:

$$\Phi(\underset{\sim}{x},t) = \sum_{k=0}^{\infty} \varphi_k(\underset{\sim}{x})\, f_{k+2}(\zeta) \tag{35a}$$

$$\underset{\sim}{\Psi}(\underset{\sim}{x},t) = \sum_{k=0}^{\infty} \underset{\sim}{\psi}_k(\underset{\sim}{x})\, f_{k+2}(\bar{\zeta}) \tag{35b}$$

where $f_o(\omega)$ is an arbitrary function of ω for $\omega \geq 0$ and vanishes for $\omega < 0$, and

$$f_{k+1}(\omega) = \int_{-\infty}^{\omega} f_k(\omega')d\omega' \tag{36a}$$

or

$$\frac{d}{d\omega} f_{k+1}(\omega) = f_k(\omega) \tag{36b}$$

Thus $f_k(\omega)$ also vanishes for $\omega < 0$ for all $k > 0$. Notice also that $f_k(0) = 0$ for all $k \geq 1$. In Eqs. (35) the terms involving f_o and f_1 are excluded because of the continuity requirement for displacements across a wave front.

The expansion expressed by Eqs. (35) has a physical meaning if we choose $f_o(\omega) = H(\omega)$, the Heaviside step function. For then $f_k(\omega) = \omega^k/k!$ and $\varphi_k(\underset{\sim}{x})$ becomes the k-th time derivative of $\Phi(\underset{\sim}{x},t)$ at the wave front $t = \tau(\underset{\sim}{x})$. Similarly, $\underset{\sim}{\psi}_k(\underset{\sim}{x})$ becomes the k-th time derivative of $\underset{\sim}{\Psi}(\underset{\sim}{x},t)$ at the wave front $t = \bar{\tau}(\underset{\sim}{x})$.

By substituting Eq. (35a) into Eq. (2) and making use of Eqs. (33a) and (36b), we obtain the higher order transport equation for φ_k in a recurrence form:

$$2(\nabla\tau)\cdot(\nabla\varphi_k) + \varphi_k \nabla^2\tau = \nabla^2\varphi_{k-1}\ , \quad (k=0,1,2,\ldots) \tag{37a}$$

provided we define $\varphi_{-1} \equiv 0$. When $k = 0$, Eq. (37a) reduces to the zero order transport equation (9). Similarly, we obtain the higher order transport equations for $\underset{\sim}{\psi}_k$ which can be written in a dyadic notation as

$$2(\nabla\bar{\tau})\cdot(\nabla\underset{\sim}{\psi}_k) + \underset{\sim}{\psi}_k \nabla^2\bar{\tau} = \nabla^2\underset{\sim}{\psi}_{k-1}\ , \quad (k=0,1,2,\ldots) \tag{37b}$$

provided we define $\underset{\sim}{\psi}_{-1} \equiv 0$.

To obtain the reflection and transmission coefficients at an interface, we have to find the displacements and stresses at the interface and apply the continuity condition. Substituting Eqs. (35) into Eq. (1) we obtain

$$\underset{\sim}{u} = \sum_{k=0}^{\infty} \left\{(\nabla\varphi_{k-1} - \varphi_k \nabla\tau) f_{k+1}(\zeta) + (\nabla \times \underset{\sim}{\psi}_{k-1} - \nabla\bar{\tau} \times \underset{\sim}{\psi}_k) f_{k+1}(\bar{\zeta})\right\} \tag{38}$$

Since $\zeta = \bar{\zeta}$ at the interface, we have

$$\underset{\sim}{u}^{b} = \sum_{k=0}^{\infty} \left\{-(\varphi_k \nabla\tau + \nabla\bar{\tau} \times \underset{\sim}{\psi}_k) + \underset{\sim}{U}_{k-1}\right\} f_{k+1}(\zeta) \tag{39}$$

where

$$\underset{\sim}{U}_{k-1} = \nabla\varphi_{k-1} + \nabla \times \underset{\sim}{\psi}_{k-1}$$

which contains only the lower order terms and a superscript b stands for the interface boundary. If we substitute Eq. (38) into the following stress-displacement relation

$$\underset{\equiv}{\sigma} = \mu(\nabla \underset{\sim}{u} + \underset{\sim}{u}\nabla) + \lambda \underset{\equiv}{I}\ \nabla \cdot \underset{\sim}{u} \tag{40}$$

and let $\zeta = \bar{\zeta}$, we obtain stresses at the boundary

$$\underset{\equiv}{\sigma}^{b} = \sum_{k=0}^{\infty} \left\{(2\mu \nabla\tau\, \nabla\tau + \frac{\lambda}{\alpha^2} \underset{\equiv}{I})\varphi_k + \mu(\nabla\bar{\tau}\, \nabla\bar{\tau} \times \underset{\sim}{\psi}_k + \nabla\bar{\tau} \times \underset{\sim}{\psi}_k \nabla\bar{\tau}) + \underset{\equiv}{S}_{k-1}\right\} f_k(\zeta) \tag{41}$$

provided we define $\varphi_{-2} \equiv 0$, $\underset{\sim}{\psi}_{-2} \equiv 0$. $\underset{\equiv}{S}_{k-1}$ contains only the lower order terms φ_{k-1}, φ_{k-2}, $\underset{\sim}{\psi}_{k-1}$, and $\underset{\sim}{\psi}_{k-2}$. Let $\underset{\sim}{n}$ and $\underset{\sim}{\bar{n}}$ be a unit vector normal to the dilatation wave front and the distortion wave front respectively. Then, by Eqs. (33),

$$\nabla\tau = \frac{1}{\alpha} \underset{\sim}{n} \tag{42a}$$

$$\nabla\bar{\tau} = \frac{1}{\beta} \underset{\sim}{\bar{n}} \tag{42b}$$

Figure 7 shows a typical configuration in which reflected and transmitted

rays are generated by an incident (Φ) ray AB or ($\underset{\sim}{\Psi}$) ray CB. Although both (Φ) ray and ($\underset{\sim}{\Psi}$) ray are drawn in the same figure, it is assumed that only one ray, AB or CB, strikes the boundary. The unusual case in which both rays strike the boundary at the same time can be obtained by considering each ray separately and superposing the results. The superscripts (i), (r) and (t) stand for incident, reflected and transmitted rays respectively. $\underset{\sim}{n}^b$ is the unit normal vector to the interface boundary at point B. Notice that all the $\underset{\sim}{n}$ and $\underset{\sim}{\bar{n}}$ vectors and $\underset{\sim}{n}^b$ lie on the same plane which is perpendicular to the boundary surface at point B. Let $\underset{\sim}{b}$ be a unit vector normal to this plane at point B and $\underset{\sim}{t}$ be a unit vector on this plane and tangent to the boundary at B so that

$$\underset{\sim}{b} = \underset{\sim}{t} \times \underset{\sim}{n}^b \tag{43}$$

$\underset{\sim}{t}$ and $\underset{\sim}{b}$ can be expressed in terms of $\underset{\sim}{n}^{(i)}$ and $\underset{\sim}{n}^{(b)}$ by

$$\underset{\sim}{t} = (\underset{\sim}{n}^{(i)} - \cos\theta\, \underset{\sim}{n}^b)/\sin\theta \tag{44a}$$

$$\underset{\sim}{b} = (\underset{\sim}{n}^{(i)} \times \underset{\sim}{n}^b)/\sin\theta \tag{44b}$$

The angles θ, $\bar{\theta}$, θ' and $\bar{\theta}'$ are related by Snell's law:

$$\frac{\alpha}{\sin\theta} = \frac{\beta}{\sin\bar{\theta}} = \frac{\alpha'}{\sin\theta'} = \frac{\beta'}{\sin\bar{\theta}'} \tag{45}$$

where a prime denotes the refracted medium. Now the condition that $\underset{\sim}{u}^b$ is continuous at point B gives, using Eqs. (39) and (42)

$$\left(\frac{1}{\alpha}\varphi_k^{(i)}\underset{\sim}{n}^{(i)} + \frac{1}{\beta}\bar{\underset{\sim}{n}}^{(i)} \times \underset{\sim}{\psi}_k^{(i)}\right) + \left(\frac{1}{\alpha}\varphi_k^{(r)}\underset{\sim}{n}^{(r)} + \frac{1}{\beta}\bar{\underset{\sim}{n}}^{(r)} \times \underset{\sim}{\psi}_k^{(r)}\right)$$

$$= \left(\frac{1}{\alpha'}\varphi_k^{(t)}\underset{\sim}{n}^{(t)} + \frac{1}{\beta'}\bar{\underset{\sim}{n}}^{(t)} \times \underset{\sim}{\psi}_k^{(t)}\right) - \underset{\sim}{U}^*_{k-1} \qquad (46)$$

$$\underset{\sim}{U}^*_{k-1} = \underset{\sim}{U}^{(t)}_{k-1} - \underset{\sim}{U}^{(i)}_{k-1} - \underset{\sim}{U}^{(r)}_{k-1}$$

The condition that the surface traction $\underline{\underline{\sigma}}^b \cdot \underset{\sim}{n}^b$ be continuous at point B gives, using Eqs. (41) ~ (44) and Fig. 7,

$$\frac{1}{\alpha^2}\left(2\mu\cos\theta\,\underset{\sim}{n}^{(i)} + \lambda\underset{\sim}{n}^b\right)\varphi_k^{(i)} + \rho\left(-Q_k^{(i)}\sin\bar{\theta}\bar{\underset{\sim}{n}}^{(i)} + \cos\bar{\theta}\,\bar{\underset{\sim}{n}}^{(i)} \times \underset{\sim}{\psi}_k^{(i)}\right)$$

$$+ \frac{1}{\alpha^2}\left(-2\mu\cos\theta\,\underset{\sim}{n}^{(r)} + \lambda\underset{\sim}{n}^b\right)\varphi_k^{(r)} + \rho\left(-Q_k^{(r)}\sin\bar{\theta}\bar{\underset{\sim}{n}}^{(r)} - \cos\bar{\theta}\,\bar{\underset{\sim}{n}}^{(r)} \times \underset{\sim}{\psi}_k^{(r)}\right)$$

$$= \frac{1}{\alpha'^2}\left(2\mu'\cos\theta'\,\underset{\sim}{n}^{(t)} + \lambda'\underset{\sim}{n}^b\right)\varphi_k^{(t)} + \rho'\left(-Q_k^{(t)}\sin\bar{\theta}'\bar{\underset{\sim}{n}}^{(t)} + \cos\bar{\theta}'\bar{\underset{\sim}{n}}^{(t)} \times \underset{\sim}{\psi}_k^{(t)}\right) + \underset{\sim}{T}^*_{k-1} \qquad (47)$$

where

$$Q_k = \underset{\sim}{\psi}_k \cdot \underset{\sim}{b} \qquad (48)$$

$$\underset{\sim}{T}^*_{k-1} = \underset{\sim}{T}^{(t)}_{k-1} - \underset{\sim}{T}^{(i)}_{k-1} - \underset{\sim}{T}^{(r)}_{k-1}$$

$$\underset{\sim}{T}_{k-1} = \underline{\underline{S}}_{k-1} \cdot \underset{\sim}{n}^b$$

If we substitute Eq. (35b) into Eq. (4) and make use of Eq. (36b), we have

$$\underset{\sim}{n}^{(r)} \cdot \underset{\sim}{\psi}_k^{(r)} = \beta \nabla \cdot \underset{\sim}{\psi}_{k-1}^{(r)} \tag{49a}$$

$$\underset{\sim}{n}^{(t)} \cdot \underset{\sim}{\psi}_k^{(t)} = \beta' \nabla \cdot \underset{\sim}{\psi}_{k-1}^{(t)} \tag{49b}$$

Equations (46) ~ (49) give a recurrence formulae for determining $\varphi_k^{(r)}$, $\varphi_k^{(t)}$, $\underset{\sim}{\psi}_k^{(r)}$ and $\underset{\sim}{\psi}_k^{(t)}$ $(k=0,1,2,\ldots)$ at the interface. Thus one can calculate, in principle, the reflection and transmission coefficients for any order of time derivatives of stress behind the wave front.

Equations (46) and (47) can be reduced to scalar equations. If we perform the scalar product on both sides of Eq. (46) by $\underset{\sim}{t}$ and $\underset{\sim}{n}^b$ respectively, we have

$$(\varphi_k^{(i)}+\varphi_k^{(r)}) + \cot\bar{\theta}\,(Q_k^{(i)}-Q_k^{(r)}) = \varphi_k^{(t)}+\cot\bar{\theta}'\,Q_k^{(t)} - \frac{\alpha}{\sin\theta}\,\underset{\sim}{U}_{k-1}^{*} \cdot \underset{\sim}{t} \tag{50}$$

$$\cot\theta\,(\varphi_k^{(i)}-\varphi_k^{(r)}) - (Q_k^{(i)}+Q_k^{(r)}) = \cot\theta'\,\varphi_k^{(t)} - Q_k^{(t)} - \frac{\beta}{\sin\bar{\theta}}\,\underset{\sim}{U}_{k-1}^{*} \cdot \underset{\sim}{n}^b \tag{51}$$

Similarly, if we perform the scalar product on both sides of Eq. (47) by $\underset{\sim}{n}^b$ and $\underset{\sim}{t}$ respectively, we obtain:

$$\mu\left\{-(\cot^2\bar{\theta}-1)(\varphi_k^{(i)}+\varphi_k^{(r)})+2\cot\bar{\theta}\,(Q_k^{(i)}-Q_k^{(r)})\right\}$$

$$= \mu'\left\{-(\cot^2\bar{\theta}'-1)\varphi_k^{(t)}+2\cot\bar{\theta}'\,Q_k^{(t)}\right\} - \frac{\beta^2}{\sin^2\bar{\theta}}\,\underset{\sim}{T}_{k-1}^{*} \cdot \underset{\sim}{n}^b \tag{52}$$

$$\mu\left\{2\cot\theta\,(\varphi_k^{(i)}-\varphi_k^{(r)})+(\cot^2\bar{\theta}-1)(Q_k^{(i)}+Q_k^{(r)})\right\}$$

$$= \mu'\left\{2\cot\theta'\,\varphi_k^{(t)}+(\cot^2\bar{\theta}'-1)Q_k^{(t)}\right\} + \frac{\beta^2}{\sin^2\bar{\theta}}\,\underset{\sim}{T}_{k-1}^{*} \cdot \underset{\sim}{t} \tag{53}$$

Finally, we perform the scalar product on both sides of Eqs. (46) and (47) by $\underset{\sim}{b}$ to obtain:

$$P_k^{(i)} + P_k^{(r)} = \frac{\beta}{\beta'} P_k^{(t)} + \beta \underset{\sim}{U}^*_{k-1} \cdot \underset{\sim}{b} \tag{54}$$

$$P_k^{(i)} - P_k^{(r)} = \frac{\rho' \cos \bar{\theta}'}{\rho \cos \bar{\theta}} P_k^{(t)} - \frac{1}{\rho \cos \bar{\theta}} \underset{\sim}{U}^*_{k-1} \cdot \underset{\sim}{b} \tag{55}$$

where

$$P_k = (\underset{\sim}{\bar{n}} \times \underset{\sim}{b}) \cdot \underset{\sim}{\Psi}_k \tag{56}$$

Equations (49) ~ (55) are alternate equations for $\varphi_k^{(r)}$, $\varphi_k^{(t)}$, $\underset{\sim}{\Psi}_k^{(r)}$ and $\underset{\sim}{\Psi}_k^{(t)}$. Notice that Q_k and P_k are the components of $\underset{\sim}{\Psi}_k$ in the $\underset{\sim}{b}$ and $\underset{\sim}{\bar{n}} \times \underset{\sim}{b}$ directions respectively while Eqs. (49) give the component of $\underset{\sim}{\Psi}_k$ in the $\underset{\sim}{\bar{n}}$ direction. Thus we have three components of $\underset{\sim}{\Psi}_k$ in three mutually orthogonal directions.

It is known that one can delete any one of the three components of $\underset{\sim}{\Psi}_k$ without loss of generality by ignoring the condition (4). In that case, Eqs. (49) which are derived from Eq. (4) are not needed and Eqs. (50) ~ (55) alone are sufficient for determining the unknowns. For two-dimensional wave motion and axially symmetric wave motion, only one component of $\underset{\sim}{\Psi}_k$, namely Q_k as defined by (48), is needed. Equations (54) and (55) are automatically satisfied and Eqs. (50) ~ (53) alone are sufficient for determining the unknowns.

It should be mentioned that Eqs. (50) ~ (53) are identical to Eqs. (3-11) ~ (3-14) of [7] for plane waves incident on plane boundary, except for the lower order terms which are zero when $k = 0$ and an

obvious difference in the use of notations. Thus the assertion that the reflection and transmission coefficients for the stress amplitudes at an interface are independent of the curvatures of the incident wave front and the interface surface has been proved. The reflection and transmission coefficients for the stress gradient and the higher order derivatives in general depend on the curvatures of the incident wave front and the interface surface through the lower order terms in Eqs. (49) ~ (55).

7. Discussion.

The analysis presented here applies to inclusions of general geometry and can be used to determine the stress behind a wave front which is reflected from an interface, a rigid surface, or a free surface. For the latter, the stress due to the incident wave should be superposed to obtain the actual stress behind the reflected wave front.

The analysis can also be applied to determine the discontinuity in shear stress across a distortion wave front. However, the geometry of the distortion wave front is in general more complicated than the dilatation wave front. Figure 8 shows some of the distortion wave fronts for the same material parameters as in Figs. 3, 5, and 6. For comparison, the dilatation wave fronts and the corresponding rays obtained in Fig. 3 are shown as dotted lines. P is the point at which the incident ray is tangential to the circumference of the inclusion. After passing point Q, there are two distortion wave fronts, one is formed by one refraction at the interface while the other is formed by reflection of

the refracted dilatation wave front inside the inclusion. The curve qs is the caustic of the reflected distortion rays and therefore shear stress becomes infinite along qs. The shear stress is also infinite at the wave front where the associated rays have touched the caustic qs. (see [2,3]). This situation does not seem to have been mentioned previously in the literature on composite materials. In fact if one considers the second dilatation wave front which is obtained from the reflection of the refracted wave front inside the inclusion, one again obtains a caustic similar to the curve qs in Fig. 8. Thus we also have an infinite stress in the inclusion due to dilatation waves. For a real material, this implies either a failure in the inclusion or the material near the curve qs becomes plastic and hence subsequent wave propagation analysis should be modified. In experiments, an infinite stress concentration along the curve qs is unlikely to happen because it is not possible to generate a truely sharp wave front as shown in Fig. 1(b). If there is a finite time for the stress to rise to its peak magnitude, an infinite stress will not occur along qs. However, this does not rule out the possibility of an infinite stress concentration occurring along other caustics which are formed by multiple reflections inside the inclusion. For instance, an incident pulse with initially continuous stress at the wave front can become, after the first reflection inside the inclusion, a shock wave front with a finite discontinuity in stress at the wave front. This shock wave front can then become a front with an infinite stress after the second reflection inside the inclusion.

It should be noted that whether the stress inside the inclusion becomes infinite or not, the solution presented in this paper concerning the leading wave front is still valid. This is obvious because of the hyperbolic nature of the wave equation considered here. The discussion presented above simply points out the fact that a complete stress analysis inside an inclusion due to the passage of a pulse is a complicated problem. When an infinite stress occurs, a realistic solution can be obtained only if one considers non-linear elastic deformation or plastic deformation.

Acknowledgements.

This work was carried out jointly at the ARPA Materials Research Council Summer Study Group and in the research program at Stanford University sponsored by the Ballistic Research Laboratories during one of the authors (TCTT) visit at Stanford University. The authors wish to express their thanks to Professors C. C. Chao of Stanford University and J. Miklowitz of the California Institute of Technology for helpful discussions during the course of this work.

References

1. Luneburg, R.D., "Mathematical Theory of Optics," University of California Press, 1964.

2. Friedlander, F. G., "Sound Pulses," Cambridge University Press, 1958, Chapters 3 and 4.

3. Friedlander, F. G., "On the Solutions of the Wave Equation with Discontinuous Derivatives," Proc. Camb. Phil. Soc. Vol. 38, 1942, pp. 378-382.

4. Friedlander, F. G., "Simple Progressive Solutions of the Wave Equation," Proc. Camb. Phil. Soc. Vol. 43, 1947, pp. 360-373.

5. Keller, J.B., and Keller, H.B.,"Determination of Reflected and Transmitted Fields by Geometrical Optics," J. Opt. Soc. Amer. Vol. 40, 1950, pp. 48-52.

6. Courant, R., and Hilbert, D., "Methods of Mathematical Physics," Vol. II. Interscience Publishers, N.Y. 1962.

7. Ewing, W.M., Jardetzky, W.S., and Press, F., "Elastic Waves in Layered Media," McGraw-Hill, New York, 1957, pp. 76-87.

8. Muskat, M., and Meres, M.W., "Reflection and Transmission Coefficients for Plane Waves in Elastic Media," Geophysics, Vol. 5, 1940, pp. 115-148.

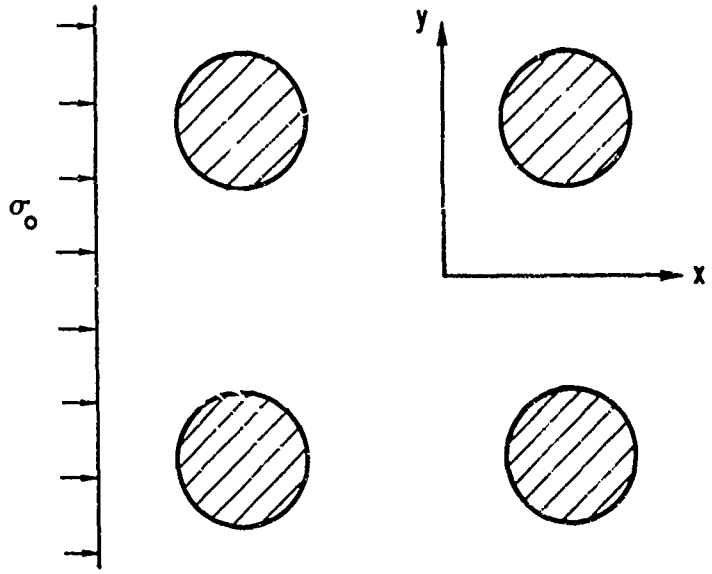

FIGURE 1(a) REINFORCING ROD CONFIGURATION

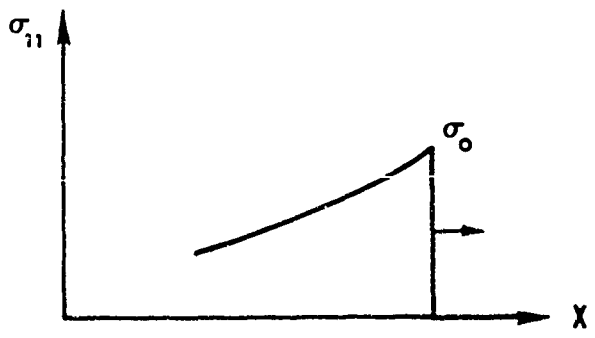

FIGURE 1(b) INITIAL NORMAL STRESS PULSE

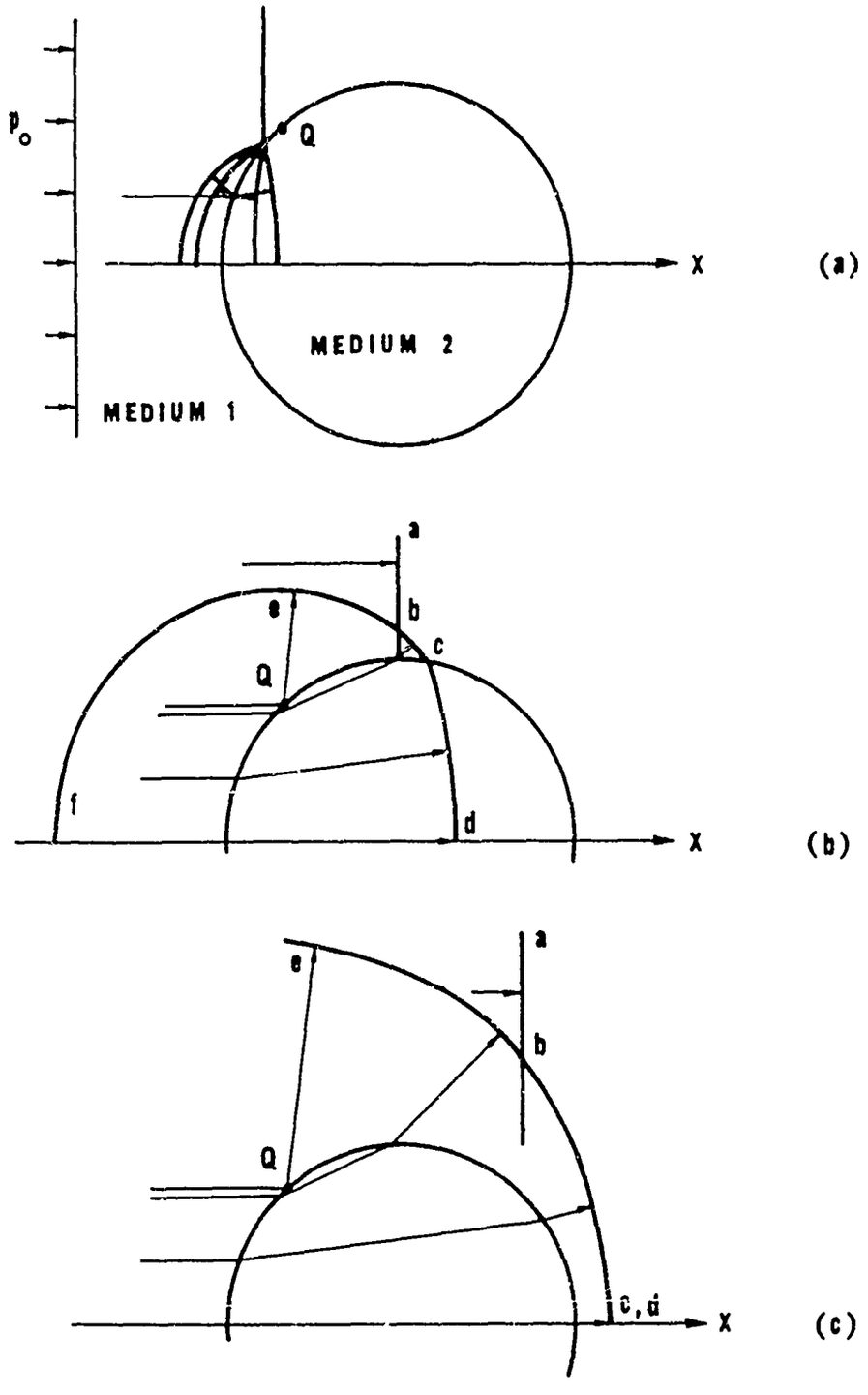

FIGURE 2 WAVE FRONT GEOMETRY $\left(\frac{\alpha_2}{\alpha_1} = \frac{4}{3}\right)$

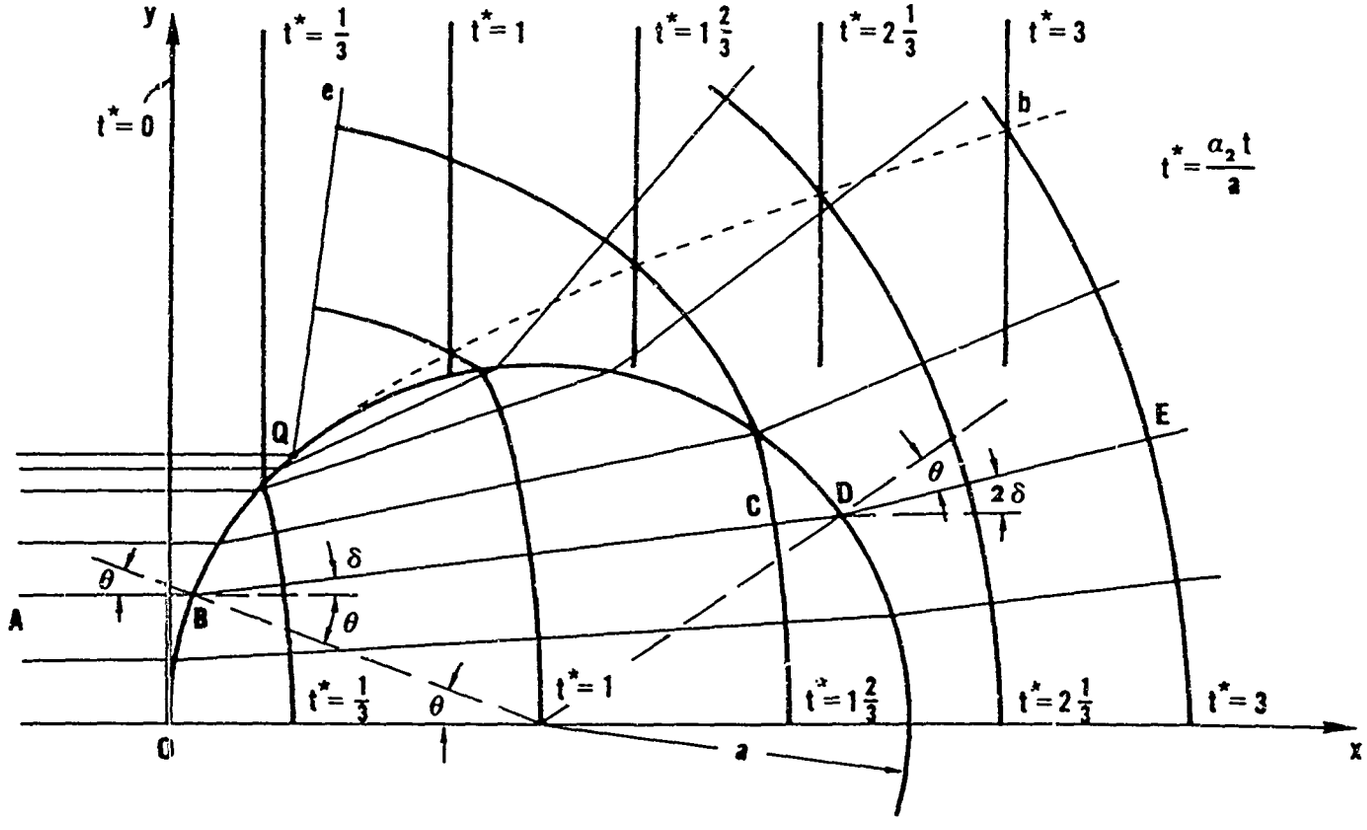

FIGURE 3 DILATATION WAVE FRONTS FOR A CIRCULAR INCLUSION

(DRAWN FOR $\frac{a_2}{a_1}=\frac{4}{3}$)

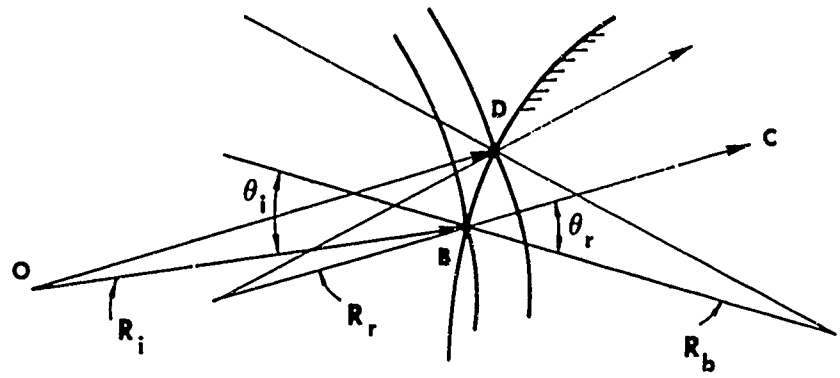

FIGURE 4 RADIUS OF CURVATURE OF A REFRACTED WAVE FRONT

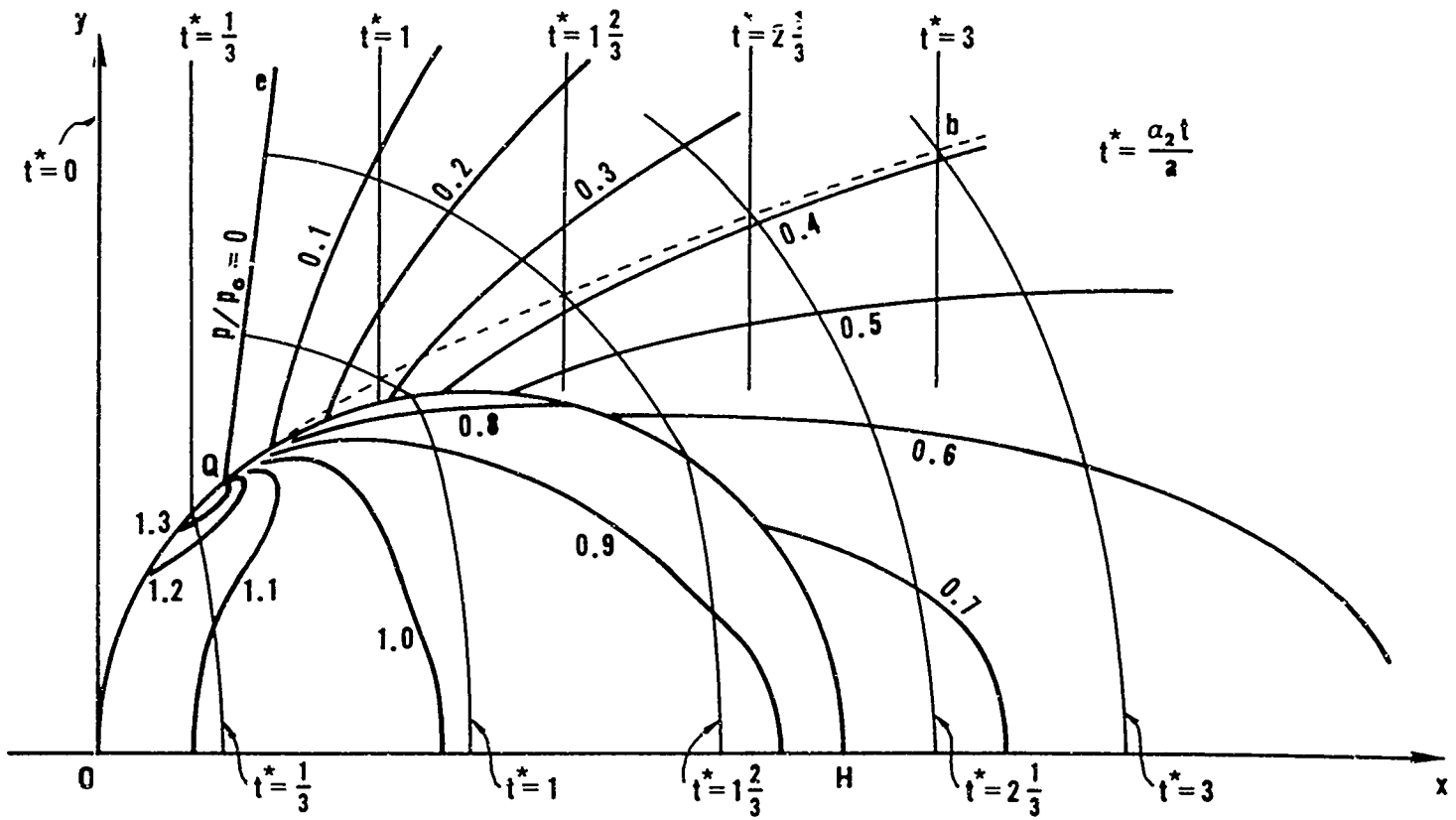

FIGURE 5 PRESSURE AT THE WAVE FRONT FOR A CYLINDRICAL INCLUSION

$\left(\text{DRAWN FOR } \frac{a_2}{a_1}=\frac{4}{3},\ \frac{\beta_1}{a_1}=\frac{\beta_2}{a_2}=\frac{1}{\sqrt{3}},\ \frac{\rho_2}{\rho_1}=1\right)$

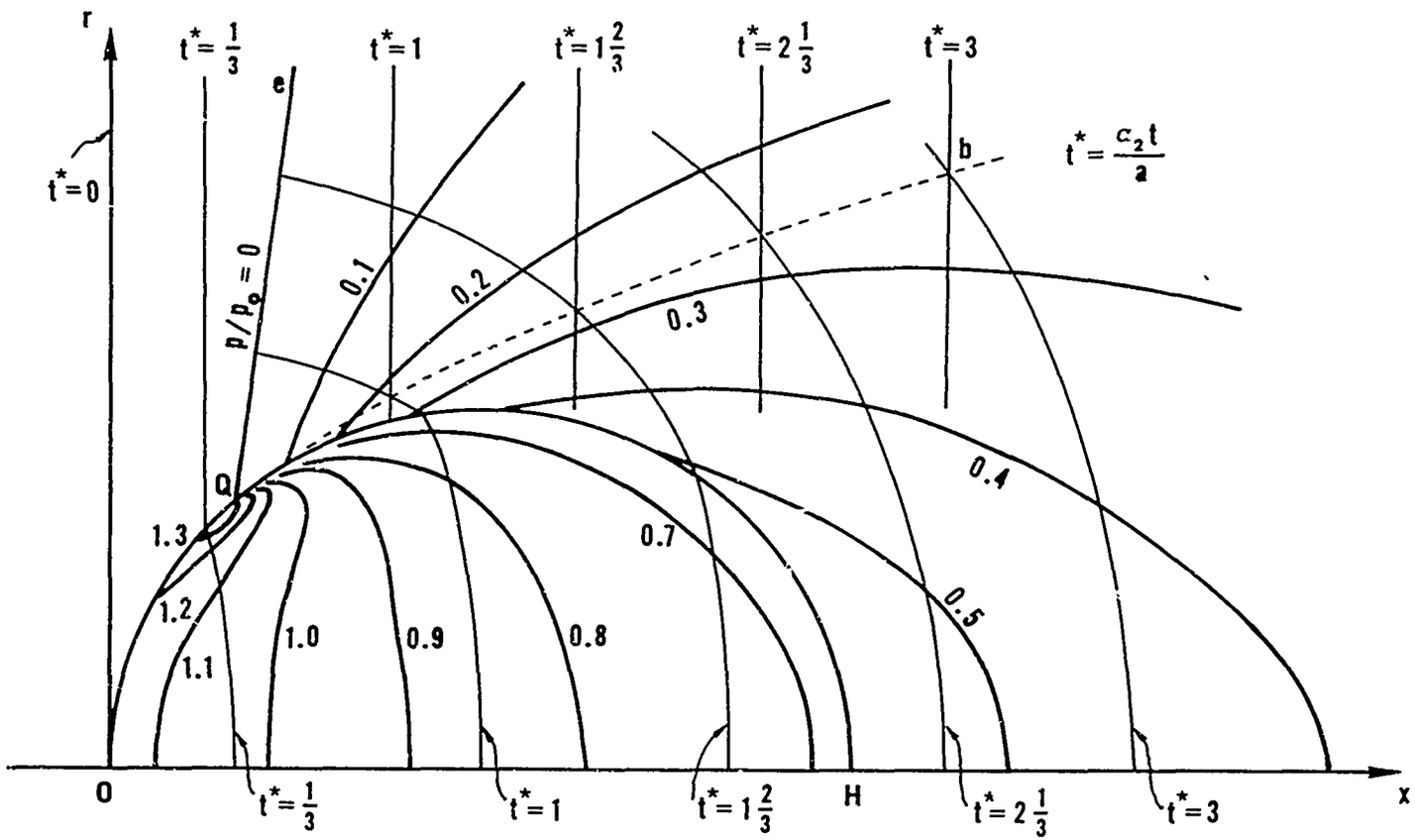

FIGURE 6 PRESSURE AT THE WAVE FRONT FOR A SPHERICAL INCLUSION

$\left(\text{DRAWN FOR } \frac{\alpha_2}{\alpha_1} = \frac{4}{3}, \quad \frac{\beta_1}{\alpha_1} = \frac{\beta_2}{\alpha_2} = \frac{1}{\sqrt{3}}, \quad \frac{\rho_2}{\rho_1} = 1\right)$

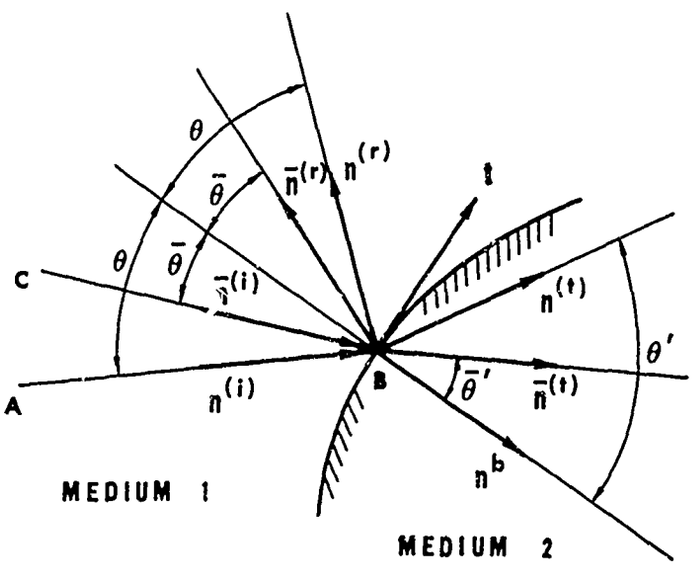

FIGURE 7 REFLECTION AND REFRACTION AT AN INTERFACE

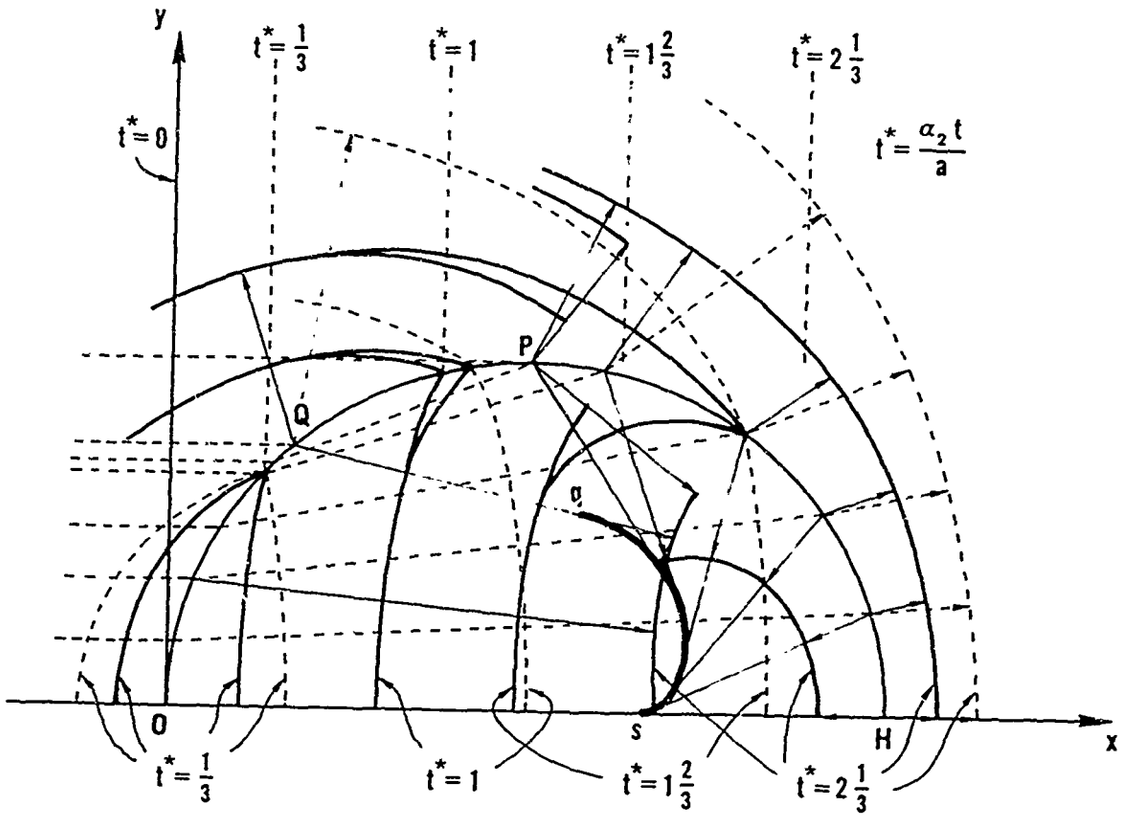

FIGURE 8 DISTORTION WAVE FRONTS FOR A CIRCULAR INCLUSION

(DRAWN FOR $\frac{\alpha_2}{\alpha_1}=\frac{4}{3}$, $\frac{\beta_1}{\alpha_1}=\frac{\beta_2}{\alpha_2}=\frac{1}{\sqrt{3}}$)

Security Classification

DOCUMENT CONTROL DATA - R & D

(Security classification of title, body of abstract and indexing annotation must be entered when the overall report is classified)

1. ORIGINATING ACTIVITY (Corporate author)	2a. REPORT SECURITY CLASSIFICATION
Department of Applied Mechanics Stanford University Stanford, Calif. 94305	Unclassified
	2b. GROUP

3. REPORT TITLE

Wave Front Analysis in Composite Materials

4. DESCRIPTIVE NOTES (Type of report and inclusive dates)

Interim Technical Report

5. AUTHOR(S) (First name, middle initial, last name)

T.C.T. Ting and E.H. Lee

6. REPORT DATE	7a. TOTAL NO. OF PAGES	7b. NO. OF REFS
December 1968	29	8

8a. CONTRACT OR GRANT NO.	9a. ORIGINATOR'S REPORT NUMBER(S)
DAHC-15-57-C-0062, No P-004 b. PROJECT NO. Materials Sc. Div., ARPA DA-04-200-AMC-659(X)	Technical Report No. 193
c.	9b. OTHER REPORT NO(S) (Any other numbers that may be assigned this report)
d.	Contract Report No. 15 [DA-659(X)]

10. DISTRIBUTION STATEMENT

Qualified requesters may obtain copies of this report from DDC

11. SUPPLEMENTARY NOTES	12. SPONSORING MILITARY ACTIVITY
None	U.S. Army, Ballistic Research Laboratories Aberdeen Proving Ground, Maryland

13. ABSTRACT

The propagation of an initially sharp plane pressure pulse through a linear elastic composite medium is analysed. Wave front and ray theory analogous to geometrical optics is shown to determine the change in shape of the leading wave front and also the stresses immediately behind it. For certain circumstances the stress amplitudes on this front, or the corresponding tensile stresses on its reflection at the free back surface of a slab, may be critical in design. Examples are presented of an initially sharp plane pressure pulse transmitted through an elastic circular cylinder and an elastic spherical inclusion. The method can be applied to more general composite configurations, and can be extended to determine the stress gradient behind the front. For the latter, general formulae are derived by which the reflection and transmission coefficients can be determined for the stress gradient and the higher order derivatives at an arbitrary interface.

DD FORM 1 NOV 65 1473

Security Classification

Security Classification

14 KEY WORDS	LINK A		LINK B		LINK C	
	ROLE	WT	ROLE	WT	ROLE	WT
Composite Materials						
Elastic Waves						
Geometrical Optics						
Geometrical Acoustics						
Elastic Inclusions						

Security Classification